Supplementary Material for "Mapping Water Flow Pathways in the Fengjiaping Landslide Using Self-Potential and Electrical Resistivity Tomography"

Kaiyan Hu[1], Qinghua Huang[2,5]*, Peng Han[3], Tao Tao[3], Shuangshuang Li[3], Shuangling Mo[3], Gexue Bai[4], Yunlong Hou[4], Ruidong Li[4], Baofeng Wan[4], Ning An[4]

[1]Hubei Subsurface Multi-Scale Imaging Key Laboratory, School of Geophysics and Geomatics, China University of Geosciences, Wuhan 430074, China.

[2]Department of Geophysics, School of Earth and Space Sciences, Peking University, Beijing 100871, China.

[3]Department of Earth and Space Sciences, Southern University of Science and Technology, Shenzhen 518055, China.

[4]Gansu Institute of Engineering Geology, Gansu Provincial Bureau of Geology and Mineral Exploration & Development, Lanzhou 730000, China.

[5]State Key Laboratory of Earthquake Dynamics and Forecasting, Peking University, Beijing 100871, China

*Corresponding author: Qinghua Huang (E-mail: huangq@pku.edu.cn)

Contents of this file

1 SP Data Processing

1.1 Electrode Preparation

Prior to deployment, all electrodes were soaked in saturated salt water for 24 h to ensure stable initial potential differences. The initial electrode voltages were recorded to monitor consistency (Fig. S1).

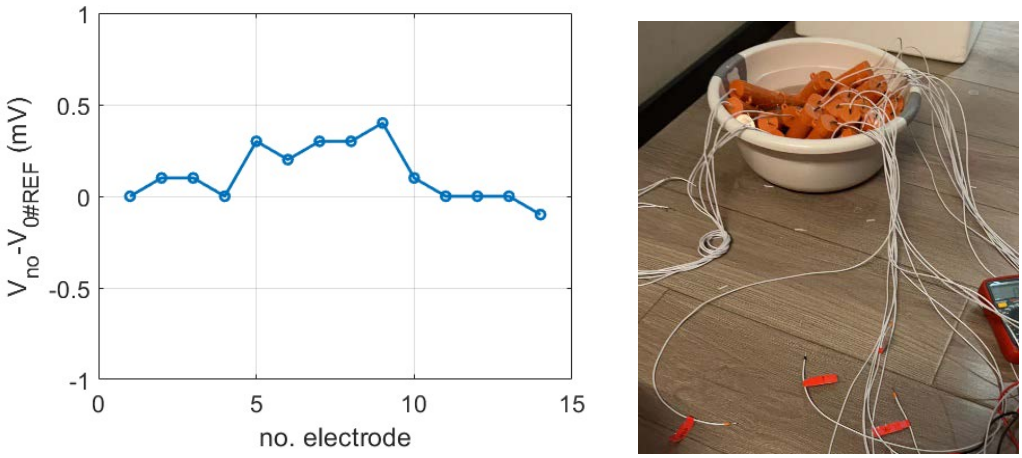

Fig. S1 The electrode voltage differences (left) soaked in salt water (right).

1.2 Field Deployment and Data Measurement

SP measurements were conducted in five subareas, as illustrated in Fig. S2. Electrodes were buried at a depth of 50 cm and allowed to stabilize for 20–30 min before measurement. The functionality of each electrode was verified using a multimeter. Multichannel SP data were then recorded under FPGA control, with each subarea referenced to its local reference electrode (yellow triangle in Fig. S2).

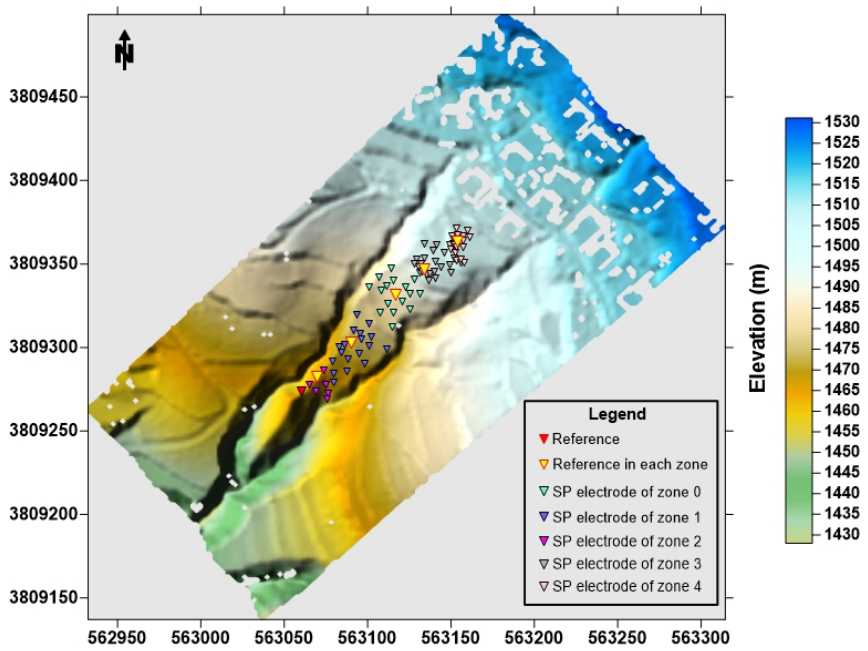

Fig. S2 SP electrodes measured in different zones

1.3 Time Series Processing

Raw SP time series were affected by ambient noise (S3a). A 1-minute moving window was applied to compute the median SP value and the corresponding standard deviation (Figs. S3c–d). The median-filtered data were used to remove initial electrode drifts (Fig. S1a). Voltage differences between reference electrodes in the five subareas were recorded to integrate all measurements relative to a common reference at the slope foot of Zone 2 (Fig. S2).

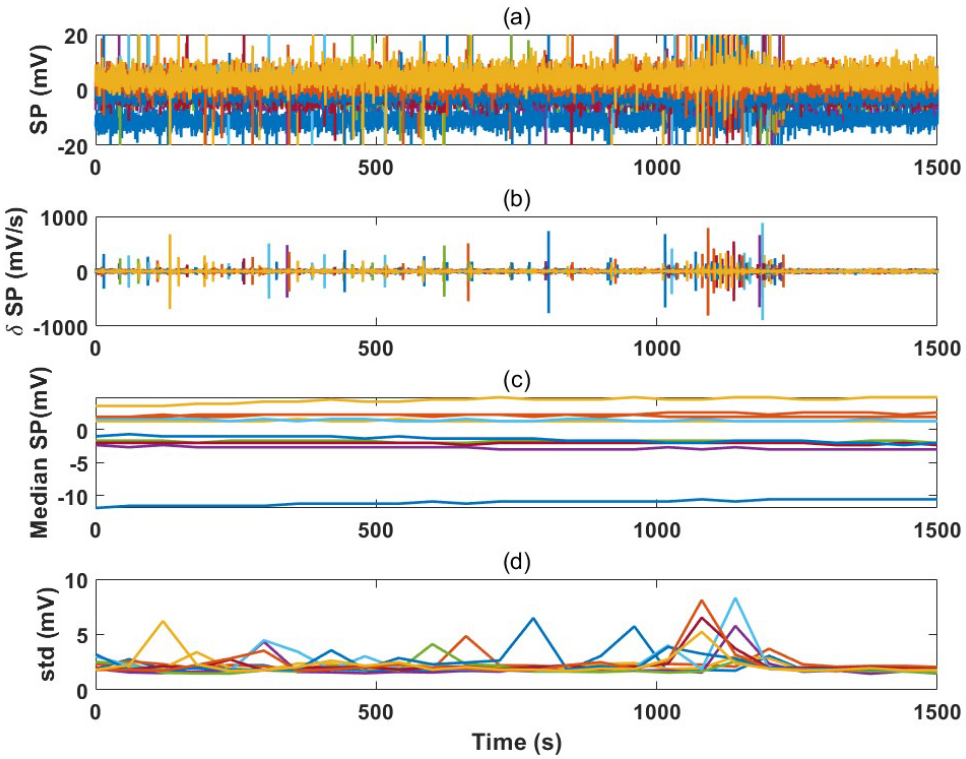

Fig. S3 The SP time series collected in Zone 3; (a) the raw data, (b) the raw SP variation rate, (c) the median SP in 1-min window; (d) the standard deviation in each minute.

1.4 Electrode details

Small non-polarizable $Pb/PbCl_2$ electrodes (type NPE121) were used, containing a gel electrolyte composed of deionized water, $PbCl_2$, HCl, NaCl, kaolinite, and nano-silicon dioxide (Fig. S4). The gel electrolyte and narrow channel design limit dehydration and electrolyte release. The electrodes exhibit a temperature drift of ~0.2 mV/°C. Temperature-induced voltage differences were corrected using measured soil temperatures at the electrode depth (Fig. S5) relative to the Zone 2 reference (Fig. S2).

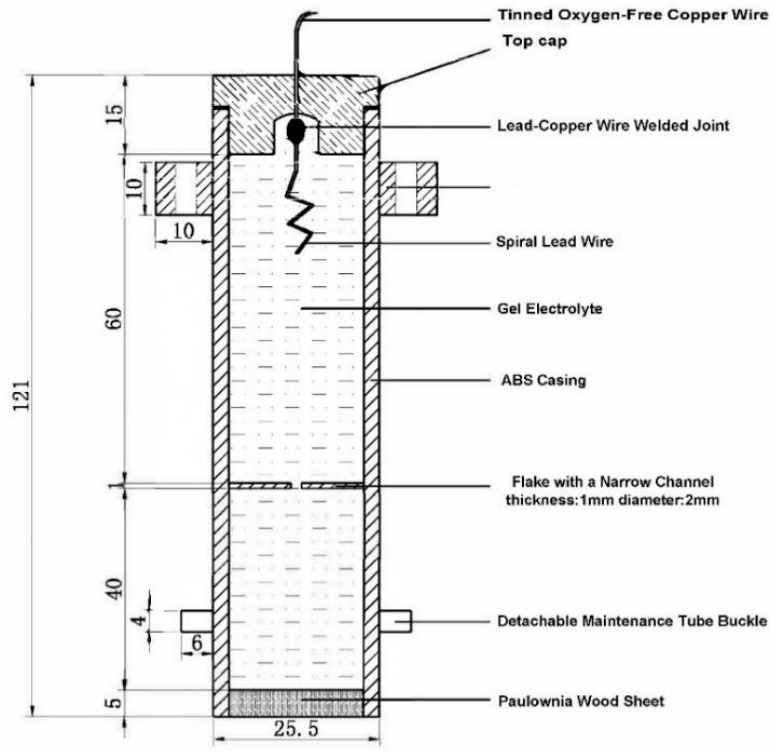

Fig. S4 The electrode structure and components (unit of length is millimeters)

Fig. S5 Photos of the sensor (left) and instrument (right) used for measuring soil parameters (SN-3001-TRREC-N01, Shandong Renke Control Technology Co., Ltd.).

1.5 SP Data for Inversion

The SP data used for inversion, located on the ERT measurement electrodes of L1, were obtained by applying natural neighbor interpolation to the three-dimensional scattered SP dataset

(Fig. S5).

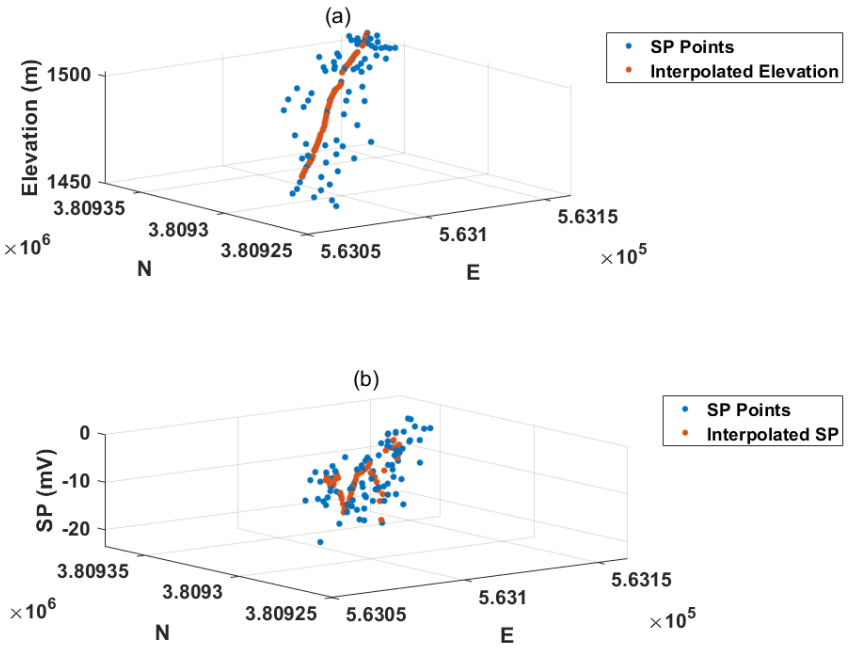

Fig. S6 SP data interpolation onto the ERT electrodes of Line 1 (L1). (a) Electrode positions: blue dots represent the original SP measurements, and orange dots indicate the ERT electrode locations where SP values were interpolated. (b) Interpolated SP values on the ERT electrodes.

2 Depth of Investigation (DOI) Assessment for ERT

We evaluated the DOI using the method proposed by Oldenburg and Li (1999) by calculating the sensitivity index $R(\mathrm{x},\mathrm{y}) = \frac{\log_{10}(\mathbf{m}_1)-\log_{10}(\mathbf{m}_2)}{\log_{10}(100)-\log_{10}(50)}$ for each survey line. Here $\mathbf{m}_1$ and $\mathbf{m}_2$ represent inversion results obtained using homogeneous initial models of 100 $\Omega \cdot \mathrm{m}$ and 50 $\Omega \cdot \mathrm{m}$, respectively. Smaller R values indicate that the inversion results have lower dependence on the initial model, reflecting higher data sensitivity and thus more reliable results. Figure S7 shows the R index variations for survey lines L2, L3, and L4, indicating that the deeper regions of the inversion results remain within the effective detection depth ($R < 0.3$). Adopting a threshold of $R = 0.3$ for the shortest survey line (L2) and $R = 0.2$ for other lines. Based on these criteria, the effective detection areas are delineated by black dashed lines. Regions outside these boundaries are strongly influenced by the initial model and are therefore considered less reliable. Overall, the deeper portions of the inversion results for L2, L3, and L4 (Fig. 6) fall within the effective DOI, whereas the shallow regions are more affected by topography and source-related singularities.

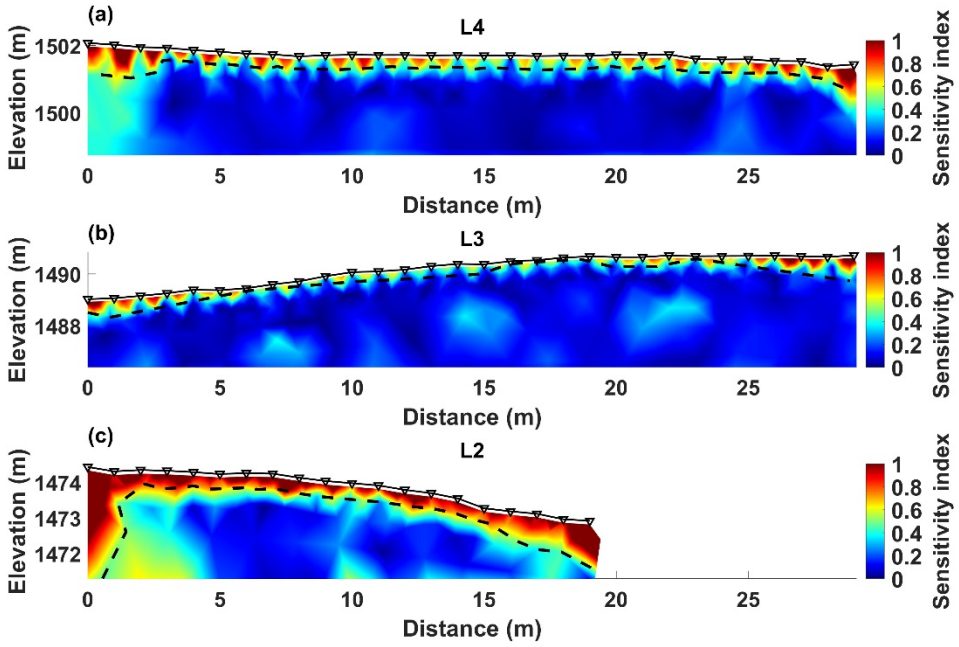

Fig. S7. Distribution of the sensitivity index (R) used to estimate the DOI for survey lines L2, L3, and L4. The black dashed line delimits the reliable imaging zone; regions above this line indicate low model dependence.

To further illustrate the spatial variation of the R index, we computed the gradient magnitude of R over the inversion mesh, defined as: $|\nabla R| = \sqrt{\left(\frac{\partial R}{\partial x}\right)^2 + \left(\frac{\partial R}{\partial z}\right)^2}$. This metric highlights region where R changes rapidly with distance or depth and thus provides complementary information on the spatial variability of inversion sensitivity. The resulting gradient maps are shown in Fig. S8, where higher values indicate areas of stronger spatial variation in the R index.

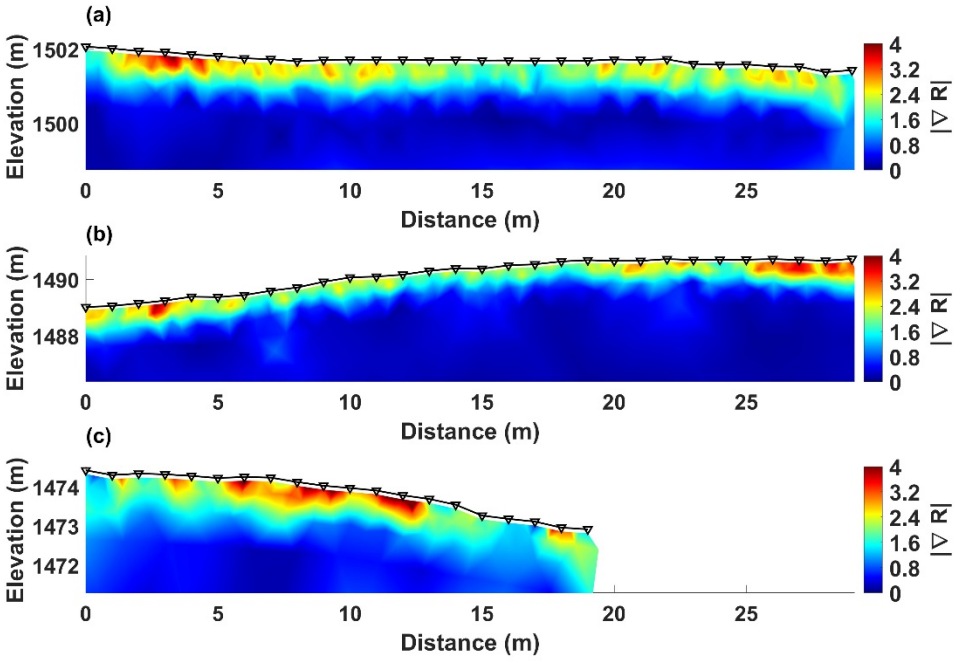

Fig. S8 Spatial variation of the R index for survey lines L2, L3, and L4

Reference:

Oldenburg, D. W., & Li, Y. (1999). Estimating depth of investigation in DC resistivity and IP surveys. Geophysics, 64(2), 403-416. https://doi.org/10.1190/1.1444545